Theoretical Study on the Potential Energy Surface for the Reaction of the Silaformyl Anion with Carbon Disulfide

Zheng-wang Qu, Ze-sheng Li,* Yi-hong Ding, and Chia-chung Sun

State Key Laboratory of Theoretical and Computational Chemistry, Institute of Theoretical Chemistry, Jilin University, Changchun 130023, People's Republic of China

Received: November 16, 1999; In Final Form: March 23, 2000

The complex potential energy surface for the ion−molecule reaction of the silaformyl anion ($HSiO^-$) with carbon disulfide (CS_2) is theoretically investigated at the B3LYP/6-311++G(d,p) level. Possible reaction channels leading to five low-lying products (**a**) $HSiOS^- + CS$, (**b**) $HCS_2^- + SiO$, (**c**) $HSiS^- + COS$, (**d**) $HCOS^- + SiS$, and (**e**) $HSiS_2^- + CO$ are probed. It is shown that all the five products are both thermodynamically and kinetically accessible via various reaction pathways involving the ion−molecule complexes and three-membered ring and four-membered ring intermediates. The calculated results significantly differ from previous experimental observation for the reaction $HSiO^- + CS_2$ that only the two products (**a**) and (**b**) were characterized, yet are in harmony with the experimental results for the isotopically labeled reaction $\mathbf{HSi^{18}O^- + CO_2}$. The large discrepancies between the theoretical and experimental results suggest that further experiments on the reaction $\mathbf{HSiO^- + CS_2}$ may be in great need. Our calculations may provide a useful guide for further identification of the three hitherto experimentally unobserved products (**c**), (**d**), and (**e**). Furthermore, the present mechanistic theoretical study may give some valuable information for other analogous ion−molecule reactions such as CH_3SiO^-, CH_3OSiO^-, $HSiS^-$, and $HSiNH^-$ with CO_2, COS, and CS_2.

1. Introduction

The chemistry of low-valent silicon-containing anions has received considerable attention from both experimentalists and theoreticians.[1] Studies of such anions in the gas phase are very helpful not only to probe their reactivity in solution where such experiments cannot be readily conducted but also to explore the chemistry and fundamental properties of the corresponding neutral silicon-containing species, which are usually highly reactive and difficult to control.

Recently, Gronert et al. prepared the silaformyl anion ($HSiO^-$) and studied its reactivity toward a variety of neutral molecules including CO_2, CS_2, COS, SO_2, O_2, CH_3CO_2H, CH_3NO_2, and C_6F_6 by using flowing afterglow selected ion flow tube (FA-SIFT) techniques.[2] They found that $HSiO^-$ possesses multiple reactive sites and has a rich ion−molecule chemistry. Among the reactions of $HSiO^-$, those with CO_2, COS, and CS_2 are of particular interest since the three neutral species are isovalently analogous and often used in mechanistic studies. Experimentally, for the reaction $HSiO^- + CO_2$, two products $HSiO_2^- + CO$ (oxygen transfer) and $HCO_2^- + SiO$ (hydride transfer) were observed with roughly equal branching ratios. The use of isotopically substituted $HSi^{18}O^-$ established that extensive oxygen−oxygen exchange between $HSiO^-$ and CO_2 took place to form five labeled and unlabeled anions, i.e., $HSi^{16}O^-$, $HSi^{18}O^{16}O^-$, $HSi^{16}O_2^-$, $HC^{18}O^{16}O^-$, and $HC^{16}O_2^-$. For the reaction $HSiO^- + COS$, four products $HSiO_2^- + CS$ (oxygen transfer), $HSiOS^- + CO$ (sulfide transfer), $HCOS^- + SiO$ (hydride transfer), and $HSiS^- + CO_2$ (oxygen−sulfide exchange) were detected with a branching ratio of trace:0.15:0.20:0.65. This indicates that the oxygen atom from $HSiO^-$ and the sulfide atom from COS undergo exchange very easily and such a process prevails over others. Also, by using the isotopically labeled anion $HSi^{18}O^-$, a small amount of oxygen−oxygen exchange product $HSi^{16}O^- + COS$ was found relative to the predominant product $HSiS^- + C^{18}O^{16}O$. Yet, the other labeled and unlabeled anions, which are associated with atom−atom exchange and atom-transfer processes, i.e., $HSi^{18}O^{16}O^-$, $HSi^{18}OS^-$, $HSi^{16}OS^-$, $HC^{18}OS^-$, and $HC^{16}OS^-$, were missing. For the analogous reaction $HSiO^- + CS_2$, similar atom-transfer products $HSiOS^- + CS$ and $HCS_2^- + SiO$ were characterized with a branching ratio of 0.30:0.70. However, to our surprise, no atom−atom exchange products were observed, although the formation of such products as $HSiS^- + COS$, $HCOS^- + SiS$, and $HSiS_2^- + CO$ might be expected. Surely, it is not parallel among the experimental results of the three analogous reactions of $HSiO^-$ with CO_2, CS_2, and COS. In order to interpret the experimental observation, Gronert et al. proposed mechanisms in which ion−molecule complexes and four-membered ring structures are involved.[2] They assumed that such mechanisms might also apply to other analogous ion−molecule reactions such as those involving CH_3SiO^-, CH_3OSiO^-,[3] $HSiS^-$, and $HSiNH^-$.[4]

Very recently, Shimizu et al. carried out a comprehensive theoretical study on the potential energy surface of the reaction $HSiO^- + CO_2$ at the MP4/6-311++G(d,p)//MP2(full)/6-31++G(d,p) level.[5] They obtained a revised mechanism that the oxygen-transfer product $HSiO_2^- + CO$ is reached via a three-membered ring intermediate instead of a four-membered ring structure as previously proposed by Gronert et al.,[2] while the four-membered ring structure is actually associated with an oxygen−oxygen exchange process between $HSiO^-$ and CO_2. Their calculated mechanism could explain the formation of four anions $HSi^{16}O^-$, $HSi^{18}O^{16}O^-$, $HC^{18}O^{16}O^-$, and $HC^{16}O_2^-$ for the isotope-labeling reaction $HSi^{18}O^- + CO_2$ with the exception of $HSi^{16}O_2^-$. Their paper highlighted the importance of carrying out accurate

* Corresponding author.

10.1021/jp9940699 CCC: $19.00
Published on Web 05/26/2000

theoretical calculations to gain mechanistic insights into gas-phase ion−molecule reactions of low-valent silicon species. To our knowledge, no theoretical investigations on the potential energy surfaces of the analogous reactions of $HSiO^-$ with CS_2 and COS have been reported.

In this paper, we decided to carry out a detailed theoretical investigation on the potential energy surface of the reaction $HSiO^- + CS_2$, since the experimental results for this reaction rather sharply contradict those for the other two analogous reactions of $HSiO^-$ with CO_2 and COS. It is obvious that the calculated mechanism for the reaction $HSiO^- + CO_2$ by Shimizu et al.[5] did not provide support for the experiment on the reaction $HSiO^- + CS_2$[2] since no atom−atom exchange product was observed in the experiment[2] whereas similar products were predicted by Shimizu et al.[5] Apparently, the potential energy surface of the reaction $HSiO^- + CS_2$ will be much more complicated than that of the reaction $HSiO^- + CO_2$. The electronegativity difference between oxygen and sulfide may also bring some thermodynamical or kinetic influences that may affect the final observed product distributions. Therefore, in order to resolve the plausible problem for the reaction $HSiO^- + CS_2$ as to whether the atom−atom exchange products $HSiS^- + COS$, $HCOS^- + SiS$, and $HSiS_2^- + CO$ could be observed or not in addition to the other two products $HSiOS^- + CS$ and $HCS_2^- + SiO$, and further to gain a deeper insight into the mechanism of the ion−molecule reactions involving $HSiO^-$, we feel that it is very desirable and useful to perform an extensive theoretical study on the reaction $HSiO^- + CS_2$.

In this paper, we employ the B3LYP/6-311++G(d,p) method to explore possible pathways leading to five products $HSiOS^- + CS$, $HCS_2^- + SiO$, $HSiS^- + COS$, $HCOS^- + SiS$, and $HSiS_2^- + CO$ for the ion−molecule reaction $HSiO^- + CS_2$. We surprisingly find that the reaction channels for all the five products are both thermodynamically and kinetically feasible, in sharp contrast to the experimental observation by Gronert et al.[2] that only the former two products were detected. However, our results are completely parallel to the experimental observation for the isotopically labeled reaction $HSi^{18}O^- + CO_2$.

2. Computational Methods

All geometries are fully optimized at the B3LYP/6-311++G-(d,p) level of theory using the GAUSSIAN 94 and GAUSSIAN 98 program packages.[6] For all stationary points, frequency calculations are performed to verify whether they are minima with all positive frequencies or transition states with only one imaginary frequency. The intrinsic reaction coordinate (IRC) calculations are further carried out at the B3LYP/6-311++G-(d,p) level to confirm that the transition state connects the right minima. The final B3LYP/6-311++G(d,p) relative energies are then corrected by including the B3LYP/6-311++G(d,p) zero-point energies (ZPE) with the total energy of the reactant $HSiO^- + CS_2$ taken as zero for reference. For simplicity, the computational level B3LYP/6-311++G(d,p) with inclusion of zero-point energy correction is abbreviated as B3LYP in this paper.

3. Results and Discussions

The B3LYP fully-optimized geometries for the reactant (R) $HSiO^- + CS_2$, 5 low-lying dissociation products (a) $HSiOS^- + CS$, (b) $HCS_2^- + SiO$, (c) $HSiS^- + COS$, (d) $HCOS^- + SiS$, and (e) $HSiS_2^- + CO$, and 25 intermediates are shown in Figure 1. The B3LYP calculated geometries for 32 transition states (TS) are depicted in Figure 2. Table 1 lists the total, relative, and zero-point vibrational energies for various structures. Then, by means of the relative energies of these structures in Table 1, an overall energetic profile of the potential energy surface (PES) for the reaction $HSiO^- + CS_2$ is presented in Figure 3. Furthermore, by means of the PES in Figure 3, the possible reaction pathways for the five products (**a**), (**b**), (**c**), (**d**), and (**e**) are obtained as shown in Figures 4, 5, 6, 7, and 8, respectively.

From the overall PES profiles of the reaction $HSiO^- + CS_2$ as shown in Figure 3, we can easily see that the microprocess of this reaction is rather complex. Starting from the energy-rich reactant (R) $HSiO^- + CS_2$, various low-lying intermediates can be reached via low-lying transition states and finally dissociate to the five products (**a**), (**b**), (**c**), (**d**), and (**e**), respectively. The calculated results in this paper are organized as follows. In section 3.1, the main features of the potential energy surface for the reaction $HSiO^- + CS_2$ involving the structural features and kinetic stability of various intermediates will be briefly described. In section 3.2, nearly all possible energetically allowed reaction channels leading to the five low-lying dissociation products (**a**), (**b**), (**c**), (**d**), and (**e**) will be presented. An overall mechanism for the reaction $HSiO^- + CS_2$ leading to the five products will then be given in section 3.3, and in section 3.4 a comparison between our calculations and the experimental results for the reaction $HSiO^- + CS_2$ will be made. Finally, the reliability of B3LYP/6-311++G(d,p) calculations will be assessed. Wherever necessary, the comparison between our calculated results for the reaction $HSiO^- + CS_2$ and the results for the reaction $HSiO^- + CO_2$ by Shimizu et al.[5] will also be provided.

3.1. Potential Energy Surface of the Reaction $HSiO^- + CS_2$. For the ion−molecule reaction $HSiO^- + CS_2$, the formation of many dissociation products may be suggested. However, we mainly consider five products, i.e., (**a**) $HSiO^- + CO_2$, (**b**) $HCS_2^- + SiO$, (**c**) $HSiS^- + COS$, (**d**) $HCOS^- + SiS$, and (**e**) $HSiS_2^- + CO$, for two reasons. First, the former two products (**a**) and (**b**) were already observed in the experiment[2] of the reaction $HSiO^- + CS_2$. Second, the analogues of the latter three were experimentally detected[2] for the reactions of $HSiO^-$ with CO_2 and COS though they were not observed for the reaction $HSiO^- + CS_2$. As shown in Table 1, all five products are energetically lower than the reactant (**R**) $HSiO^- + CS_2$ with the respective relative energies being −10.3, −22.5, −24.0, −25.6, and −62.6 kcal/mol. Notice that the experimentally unobserved products (**c**), (**d**), and (**e**) lie below the observed ones (**a**) and (**b**). In addition, two products (**f**) $HCO^- + SiS_2$ and (**g**) $HCS^- + SiOS$ are preliminarly calculated in this paper. Yet, their relative energies are so high (30.8 and 41.3 kcal/mol above that of the reactant (**R**) for (**f**) and (**g**), respectively) that surely both cannot compete with the five low-lying products (**a**), (**b**), (**c**), (**d**), and (**e**) thermodynamically. Thus, the products (**f**) and (**g**) will not be considered further.

From Figure 3 and Table 1, we also know that on the potential energy surface of the reaction $HSiO^- + CS_2$ all 25 intermediate structures considered in this paper lie energetically below the reactant (**R**) $HSiO^- + CS_2$. According to the geometrical features as shown in Figure 1, the 25 structures can be classified into four groups, i.e., ion−molecule complexes (**a**, **b**, **d**, **g**, **g′**, **i**, **j**, **k**, **l**, **l′**, **m**, **m′**, **r**, **u**, and **v**), three-membered ring (**c**, **f**, and **h**), four-membered ring (**e**, **o**, **p**, and **q**), and multicyclic (**n**, **s**, and **t**) intermediates. Note that **g′**, **l′**, and **m′** are the corresponding cis−trans isomers of **g**, **l**, and **m**. Furthermore, we can obtain that most of the transition states connecting the 25 intermediates

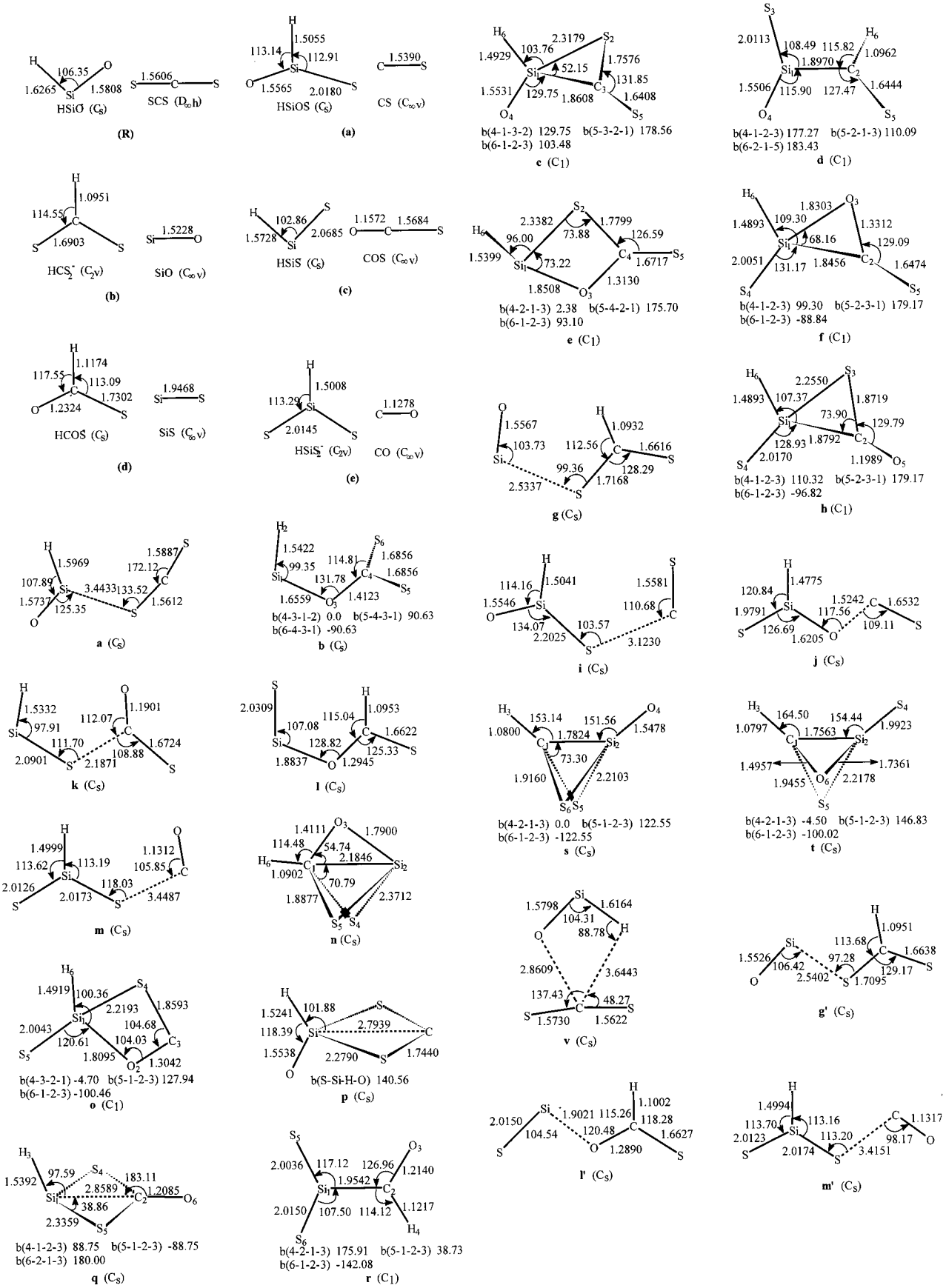

Figure 1. Geometries of the reactants, products, and intermediates at the B3LYP/6-311++G(d,p) level. Bond lengths are in angstroms and bond angles in degrees.

are lower in energy than the reactant (**R**) $HSiO^- + CS_2$. The exceptions are **TScg**, **TSel**, **TSeo**, **TSps**, and **TSpq** whose relative energies are 0.5, 3.6, 27.3, 22.1, and 22.5 kcal/mol above that of the reactant, respectively. In addition, two degenerate transition states **TScc** and **TSee**, which are associated with the self-exchange of **c** and **e**, respectively, are obtained. By making

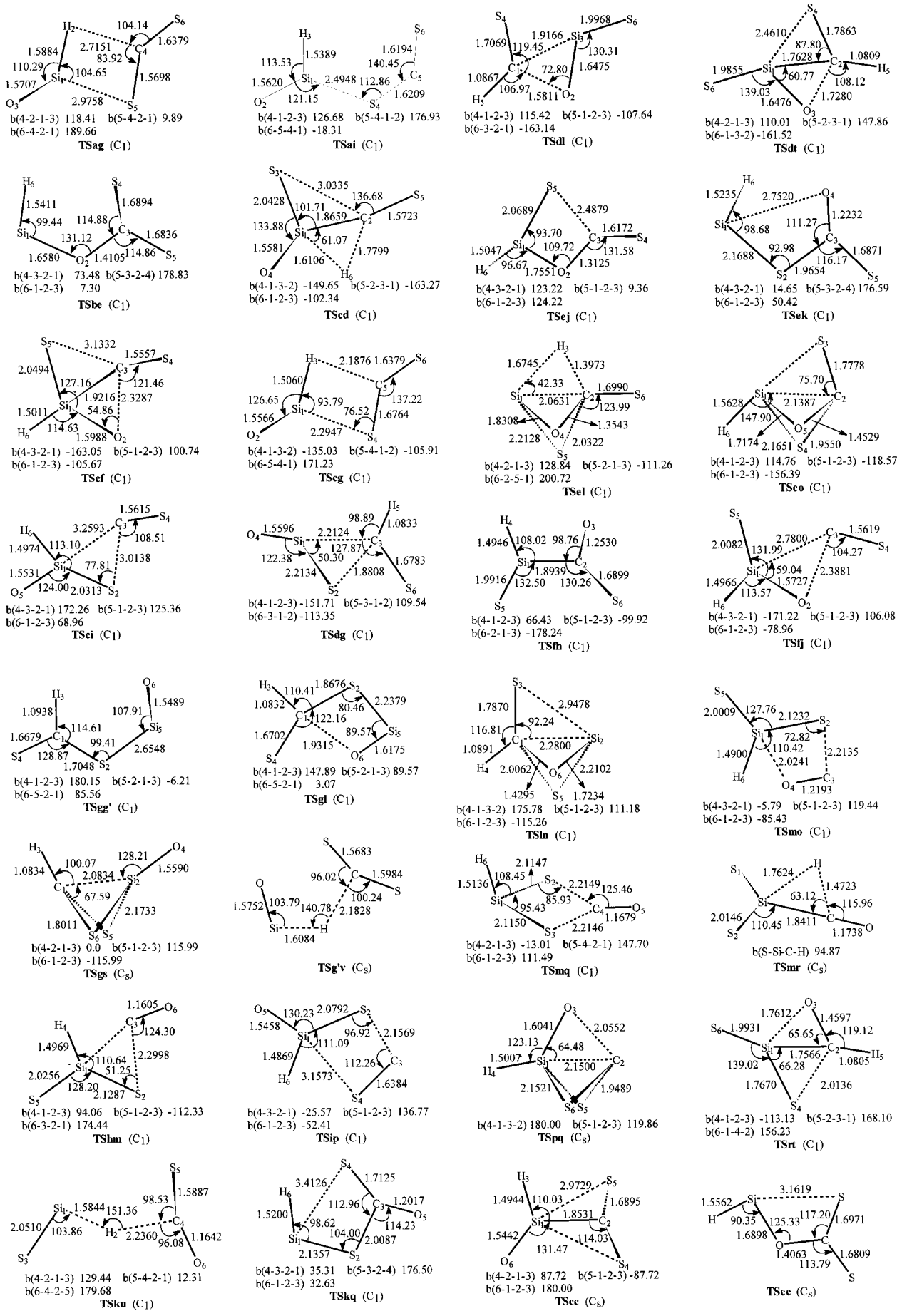

Figure 2. Geometries of the transition states at the B3LYP/6-311++G(d,p) level. Bond lengths are in angstroms and bond angles in degrees.

TABLE 1: Total Energies without (*E*, in au) and with (TE, in au) Zero-Point Vibration Energies (ZPVE, in au) and Relative Energies (RE, in kcal/mol) of the Reactants, Intermediates, Transition States, and Products Calculated at the B3LYP/6-311++G(d,p) Level of Theory

species	*E* (au)	ZVPE (au)	TE (au)	RE (kcal/mol)
(R) $HSiO^- + CS_2$	−1199.942 784	0.014 499	−1199.928 285	0.0
a	−1199.953 624	0.015 065	−1199.938 559	−6.4
b	−1199.971 212	0.018 178	−1199.953 034	−15.5
c	−1200.013 550	0.019 224	−1199.994 326	−41.4
d	−1200.033 747	0.021 292	−1200.012 454	−52.8
e	−1200.007 667	0.019 471	−1199.988 196	−37.6
f	−1200.023 319	0.019 881	−1200.003 438	−47.2
g	−1200.019 972	0.021 309	−1199.998 663	−44.2
g′	−1200.019 894	0.020 978	−1199.998 916	−44.3
h	−1200.036 348	0.019 488	−1200.016 860	−55.6
i	−1199.961 349	0.016 177	−1199.945 172	−10.6
j	−1199.964 970	0.017 195	−1199.947 775	−12.2
k	−1199.987 466	0.017 629	−1199.969 837	−26.1
l	−1200.037 453	0.022 366	−1200.015 087	−54.5
l′	−1200.035 021	0.022 205	−1200.012 817	−53.0
m	−1200.046 554	0.016 741	−1200.029 812	−63.7
m′	−1200.046 599	0.016 736	−1200.029 863	−63.7
n	−1199.985 313	0.022 638	−1199.962 675	−21.6
o	−1200.009 105	0.019 072	−1199.990 033	−38.7
p	−1199.984 126	0.018 400	−1199.965 726	−23.5
q	−1200.018 118	0.019 313	−1199.998 805	−44.3
r	−1200.051 591	0.021 563	−1200.030 028	−63.8
s	−1199.995 536	0.021 540	−1199.973 996	−28.7
t	−1199.984 281	0.021 430	−1199.962 851	−21.7
u	−1200.036 336	0.021 936	−1200.014 406	−54.0
v	−1199.949 680	0.015 528	−1199.934 152	−3.7
(a) $HSiOS^- + CS$	−1199.960 270	0.015 596	−1199.944 676	−10.3
(b) $HCS_2^- + SiO$	−1199.983 404	0.019 275	−1199.964 129	−22.5
(c) $HSiS^- + COS$	−1199.982 720	0.016 150	−1199.966 568	−24.0
(d) $HCOS^- + SiS$	−1199.988 875	0.019 852	−1199.969 023	−25.6
(e) $HSiS_2^- + CO$	−1200.044 371	0.016 272	−1200.028 099	−62.6
(f) $HCO^- + SiS_2$	−1199.893 060	0.013 810	−1199.879 250	30.8
(g) $HCS^- + SiOS$	−1199.878 488	0.016 064	−1199.862 424	41.3
(R) $HSiO^- + CS_2$	−1199.942 784	0.014 499	−1199.928 285	0.0
TSag	−1199.951 182	0.015 844	−1199.935 338	−4.4
TSai	−1199.946 418	0.016 099	−1199.930 319	−1.3
TSbe	−1199.971 188	0.018 177	−1199.953 011	−15.5
TScc	−1200.005 359	0.018 501	−1199.986 858	−36.8
TScd	−1199.962 648	0.016 349	−1199.946 299	−11.4
TScf	−1199.972 977	0.018 046	−1199.954 931	−16.7
TScg	−1199.944 315	0.016 751	−1199.927 564	0.5
TSci	−1199.960 728	0.016 411	−1199.944 317	−10.1
TSdg	−1199.976 241	0.020 654	−1199.955 587	−17.1
TSdl	−1199.987 061	0.021 523	−1199.965 538	−23.4
TSdt	−1199.981 769	0.020 906	−1199.960 864	−20.4
TSee	−1199.969 084	0.017 702	−1199.951 383	−14.5
TSej*	−1199.942 659			0.0
TSek	−1199.973 836	0.017 833	−1199.956 003	−17.4
TSel	−1199.939 995	0.017 471	−1199.922 525	+3.6
TSeo	−1199.901 421	0.016 632	−1199.884 788	+27.3
TSfh	−1200.014 588	0.018 676	−1199.995 912	−42.4
TSfj	−1199.961 839	0.016 574	−1199.945 265	−10.7
TSgg′	−1200.013 424	0.020 494	−1199.992 930	−40.6
TSgl	−1199.983 035	0.021 296	−1199.961 738	−21.0
TSgs	−1199.969 978	0.020 612	−1199.949 366	−13.2
TSg'v	−1199.948 758	0.015 733	−1199.933 025	−3.0
TShm	−1200.033 643	0.018 904	−1200.014 739	−54.3
TSip	−1199.951 207	0.016 538	−1199.934 669	−4.0
TSku	−1199.985 065	0.016 429	−1199.968 637	−25.3
TSkq	−1199.979 094	0.017 763	−1199.961 332	−20.7
TSln	−1199.979 476	0.022 201	−1199.957 275	−18.2
TSmr	−1200.007 351	0.017 241	−1199.990 110	−38.8
TSmq	−1199.970 818	0.017 511	−1199.953 307	−15.7
TSmo	−1200.004 602	0.018 063	−1199.986 539	−36.6
TSpq	−1199.909 413	0.016 963	−1199.892 450	+22.5
TSrt	−1199.984 233	0.021 088	−1199.963 145	−21.9

use of the transition states and dissociation products, we can then discuss the kinetic stability of these intermediates toward isomerization and dissociation. The kinetic properties of these species may be useful for discussion of the channels and mechanism for the reaction $HSiO^- + CS_2$ as presented in sections 3.2 and 3.3.

The ion−molecule complexes **d**, **g**, **l**, **r**, and **u** are not only energetically rather low-lying but also are kinetically very stable.

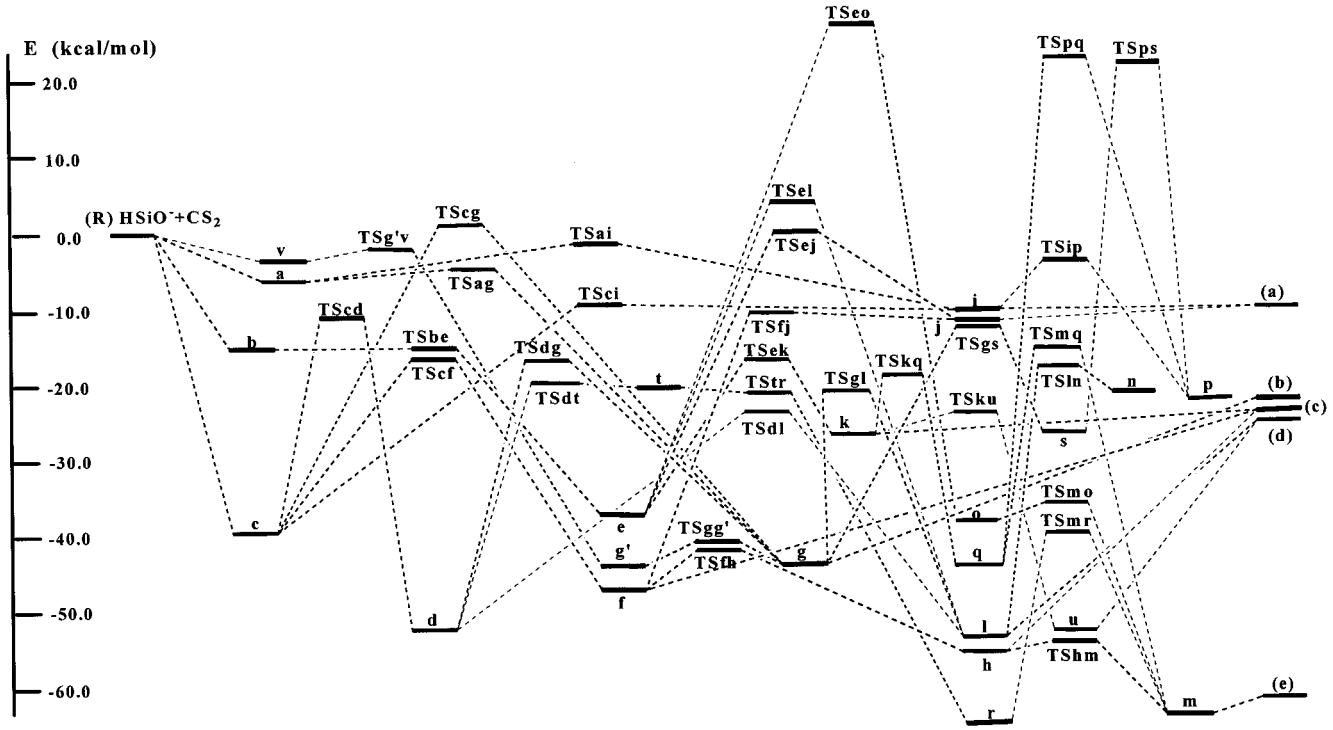

Figure 3. Profile of potential energy surface for the reaction $HSiO^- + CS_2$ at the B3LYP/6-311++G(d,p) level with inclusion of zero-point vibration energy correction.

Path (a1) (R)→a→i→(a)
Path (a2) (R)→a (v)→g (g')→l→d→c→i→(a)
Path (a3) (R)→a (v)→g (g')→l→d→c→f→j→(a)
Path (a4) (R)→a (v)→g (g')→l→d→t→r→m→h→f→j→(a)
Path (a5) (R)→a (v)→g (g')→d→c→i→(a)
Path (a6) (R)→a (v)→g (g')→d→c→f→j→(a)
Path (a7) (R)→a (v)→g (g')→d→t→r→m→h→f→j→(a)
Path (a8) (R)→b→e→k→q→m→h→f→j→(a)
Path (a9) (R)→b→e→k→q→m→r→t→d→c→f→j→(a)
Path (a10) (R)→b→e→k→q→m→r→t→d→c→i→(a)
Path (a11) (R)→c→i→(a)
Path (a12) (R)→c→f→j→(a)
Path (a13) (R)→c→d→t→r→m→h→f→j→(a)

Figure 4. Possible reaction pathways for product (**a**) $HSiOS^-$ + CS.

Path (b1) (R)→a (v)→g (g')→(b)
Path (b2) (R)→b→e→k→q→m→h→f→c→d→g→(b)
Path (b3) (R)→b→e→k→q→m→h→f→c→d→l→g→(b)
Path (b4) (R)→b→e→k→q→m→r→t→d→g→(b)
Path (b5) (R)→b→e→k→q→m→r→t→d→l→g→(b)
Path (b6) (R)→c→d→g→(b)
Path (b7) (R)→c→d→l→g→(b)
Path (b8) (R)→c→f→h→m→r→t→d→g→(b)
Path (b9) (R)→c→f→h→m→r→t→d→l→g→(b)

Figure 5. Possible reaction pathways for product (**b**) HCS_2^- + SiO.

Their corresponding relative energies are −52.8, −44.2, −54.4, −63.8, and −54.0 kcal/mol and their least isomerization or dissociation barriers are 29.4 (**d** → **i**), 21.7 (**g** → (**b**)), 28.9 (**l** → (**d**)), 25.0 (**r** → **m**), and 28.4 (**u** → (**d**)) kcal/mol, respectively. Notice that the cis−trans isomers **g** and **g′** can easily convert to each other with the barrier of only about 5 kcal/mol. The ion−molecule species **a** (−6.4), **b** (−15.5), **i** (−12.2), **k** (−26.1), **m** (−63.7), and **v** (−3.7), however, are kinetically quite unstable since their least conversion barriers are only 2.0 (**a** → **g**), 0.0 (**b** → **e**), 0.3 (**i** → (**a**)), 1.5 (**j** → **f**), 0.8

Path (c1) (R)→a (v)→g (g')→d→c→f→(c)
Path (c2) (R)→a (v)→g (g')→d→c→f→h→(c)
Path (c3). (R)→a (v)→g (g')→d→c→f→h→m→q→k→(c)
Path (c4) (R)→a (v)→g (g')→d→t→r→m→h→(c)
Path (c5) (R)→a (v)→g (g')→d→t→r→m→h→f→(c)
Path (c6) (R)→a (v)→g (g')→d→t→r→m→q→k→(c)
Path (c7) (R)→a (v)→g (g')→l→d→c→f→(c)
Path (c8) (R)→a (v)→g (g')→l→d→c→f→h→(c)
Path (c9) (R)→a (v)→g (g')→l→d→c→f→h→m→q→k→(c)
Path (c10) (R)→a (v)→g (g')→l→d→r→m→h→(c)
Path (c11) (R)→a (v)→g (g')→l→d→t→r→m→h→f→(c)
Path (c12) (R)→a (v)→g (g')→l→d→m→q→k→(c)
Path (c13) (R)→b→e→k→(c)
Path (c14) (R)→b→e→k→q→m→h→(c)
Path (c15) (R)→b→e→k→q→m→h→f→(c)
Path (c16) (R)→b→e→k→q→m→r→t→d→c→f→(c)
Path (c17) (R)→b→e→k→q→m→r→t→d→c→f→h→(c)
Path (c18) (R)→c→f→(c)
Path (c19) (R)→c→f→h→(c)
Path (c20) (R)→c→f→h→m→q→k→(c)
Path (c21) (R)→c→d→t→r→m→h→(c)
Path (c22) (R)→c→d→t→r→m→h→f→(c)
Path (c23) (R)→c→d→t→r→m→q→k→(c)

Figure 6. Possible reaction pathways for product (**c**) $HSiS^-$ + COS.

(**k** → **u**), 1.1 (**m** → (**e**)), and 0.7 (**v** → **g**) kcal/mol, respectively. The structures **g′**, **l′**, and **m′** almost have the same relative energies as their cis−trans counterparts and may have similar kinetic stability; i.e., **g′** and **l′** are kinetically stable, whereas **m′** is kinetically unstable. Of course, the cis−trans conversion barriers between these structures are expected to be small. For example, the cis−trans conversion barrier between **g** and **g′** is calculated to be only about 5 kcal/mol.

Three kinds of three-membered ring structures **c** (−41.4), **f** (−47.2), and **h** (−55.6) are obtained in this paper. The species **c** and **h** each have a SiSC three-membered ring, while **f**

Path (d1) (R)→a (v)→g (g')→l→(d)

Path (d2) (R)→a (v)→g (g')→d→l→(d)

Path (d3) (R)→a (v)→g (g')→d→t→r→m→q→k→u→(d)

Path (d4) (R)→a (v)→g (g')→d→c→f→h→m→q→k→u→(d)

Path (d5) (R)→b→e→k→u→(d)

Path (d6) (R)→b→e→k→q→m→h→f→c→d→g→l→(d)

Path (d7) (R)→b→e→k→q→m→h→f→c→d→l→(d)

Path (d8) (R)→b→e→k→q→m→r→t→d →l→(d)

Path (d9) (R)→b→e→k→q→m→r→t→d→g→l→(d)

Path (d10) (R)→c→d→l→(d)

Path (d11) (R)→c→d→g→l→(d)

Path (d12) (R)→c→d→t→r→m→q→k→u→(d)

Path (d13) (R)→c→f→h→m→q→k→u→(d)

Path (d14) (R)→c→f→h→m→r→t→d→l→(d)

Figure 7. Possible reaction pathways for product (**d**) $HCOS^-$ + SiS.

Path (e1) (R)→a (v)→g (g')→d→c→f→h→m→(e)

Path (e2) (R)→a (v)→g (g')→d→t→r→m→(e)

Path (e3) (R)→a (v)→g (g')→l→d→c→f→h→m→(e)

Path (e4) (R)→a (v)→g (g')→l→d→t→r→m→(e)

Path (e5) (R)→b→e→k→q→m→(e)

Path (e6) (R)→c→f→h→m→(e)

Path (e7) (R)→c→d→t→r→m→(e)

Figure 8. Possible reaction pathways for product (**e**) $HSiS_2^-$ + CO.

possesses a SiOC three-membered ring. The three species can be converted to each other successively through a concerted ring open and ring closure mechanism via two transition states **TScf** and **TSfh**. From Table 1, we know that only **c** is kinetically stable with the least barrier 24.7 kcal/mol toward isomerization to **f**, while **f** and **h** are both kinetically unstable since their respective least stabilization barriers are just 4.8 (**f** → **h**) and 1.3 (**h** → **m**) kcal/mol although **f** and **h** are energetically very low-lying. Thus, along the sequence **c** → **f** → **h**, the thermodynamical stability increases whereas the kinetic stability decreases.

Four intermediates **e** (−37.6), **o** (38.7), **p** (23.5), and **q** (−44.3) are suitable for four-membered ring description among which **e** and **o** possess SiOCS four-membered rings with respective exocyclic C−S and Si−S bonding while **p** and **q** possess SiSCS four-membered rings with respective exocyclic Si−O and C−O bonding. Notice that for all the four species, the H atom is bonded to the Si atom. Their least conversion barriers are 20.2 (**e** → **k**), 2.1 (**o** → **m**), 19.5 (**p** → **q**), and 23.6 (**q** → **k**) kcal/mol, respectively. Therefore, **e**, **p**, and **q** are kinetically stable, whereas **o** is kinetically unstable.

The structures **n** (−21.6), **s** (−28.7), and **t** (−21.7) are best described as multicyclic intermediates since **n** possesses three three-membered rings while **s** and **t** possess two three-membered rings. The species **n** and **t** are kinetically unstable since their least conversion barriers are just 3.4 (**n** → **l**) and −0.2 (**t** → **r**), respectively. The negative barrier from **t** to **r** actually indicates that structure **t** may disappear at higher levels. Structure **s** has a moderate barrier of 15.5 kcal/mol toward isomerization to structure **p**.

3.2. Reaction Channels for Products (a), (b), (c), (d), and (e). From Figure 3, we know that starting from the reactant (**R**) $HSiO^- + CS_2$, three weakly bound ion−molecule complexes **a**, **b**, and **v** and one kinetically stable three-membered ring structure **c** can be initially formed with no barrier. Subsequently, successive isomerization of the four species via various reaction pathways can lead to the five products (**a**), (**b**), (**c**), (**d**), and (**e**). For the formation of each product, many possible pathways may have a contribution, as shown in Figures 4, 5, 6, 7, and 8, respectively. The possible pathways for the observed products (**a**) and (**b**) are discussed in section 3.2.1, while those for the unknown products (**c**), (**d**), and (**e**) are discussed in section 3.2.2. Notice that the pathways with higher-energy transition states than that of the reactant are not presented.

3.2.1. Formation of (a) $HSiOS^-$ + CS and (b) HCS_2^- + SiO. The products (**a**) and (**b**), which are associated with the respective sulfide-transfer and hydride-transfer processes, were experimentally observed by Gronert et al.[2] By means of the PES for the reaction $HSiO^- + CS_2$ as shown in Figure 3, we can obtain 13 possible pathways for product (**a**) and nine for product (**b**) as shown in Figures 4 and 5, respectively.

All the transition states and intermediates involved in the pathways presented in Figures 4 and 5 are energetically lower than the reactant (**R**). Thus, in principle, all these pathways may contribute more or less to the formation of the products (**a**) and (**b**). In section 3.1, we know that the species **f** (three-membered ring), **h** (three-membered ring), and **m** (ion−molecule complex) are kinetically unstable with the respective least conversion barriers of 4.8 (**f** → **h**), 1.3 (**h** → **m**), and 1.1 (**m** → (**e**)) kcal/mol. On the other hand, their least conversion barriers to other intermediates or dissociation products are 24.0 (**f** → (**c**)), 13.2 (**h** → **f**), and 9.4 (**m** → **h**) kcal/mol, respectively. Furthermore, the three species lie well below the reactant (**R**) with the corresponding relative energies of −47.2, −55.6, and −63.7 kcal/mol. This indicates that once the three species are formed, the large exothermicity released may propel the successive isomerization from **f** to **h** and **h** to **m** very rapidly followed by the final dissociation of **m** to the lowest-lying product (**e**). Therefore, the contribution of the reaction pathways involving one or more of the three species **f**, **h**, and **m** seems very unimportant for the formation of the products (**a**) and (**b**). Then, the pathways of path (**a3**, **a4**, **a6**, **a7**, **a8**, **a9**, **a10**) and path (**b2**, **b3**, **b4**, **b5**, **b8**, **b9**) can be considered just as "feasible", whereas those of path (**a1**, **a2**, **a5**, **a11**) and path (**b1**, **b6**, **b7**) as "more feasible". For clarity, the more feasible pathways are underlined in Figures 4, 5, 6, 7, and 8. In the following parts, our attention will be focused on these more feasible pathways.

Among the four more feasible pathways for product (**a**), path (**a1**) and path (**a11**), which involve the initial intermediates **a** and **c**, respectively, are the simplest ones providing two "direct" sulfide-transfer routes from CS_2 to $HSiO^-$. Path (**a2**) and path (**a5**), however, are more complex both involving the initially formed species **a** or **v**. In addition to the species **c** and **i**, the low-lying and kinetically stable ion−molecule complexes **g** (or **g′**), **l**, and **d** are involved in both pathways. Since the barrier from **a** to **i** is 3.1 kcal/mol higher than that from **a** to **g**, path (**a1**) may be somewhat less competitive than path (**a2**) and path (**a5**). Also, path (**a2**) seems a little more competitive than path (**a5**) since the energy of **TSgl** is 3.9 kcal/mol lower than that of **TSdg**. Yet, the competition between path (**a2**, **a5**) and path (**a11**) is difficult to predict without dynamic calculations.

For the formation of product (**b**), the final intermediate prior to dissociation is the species **g** and **g′**. The simplest route is path (**b1**) in which only two ion−molecule complexes **a** and **g** (or **v** and **g′**) are involved. In path (**b6**), the initially formed three-membered ring structure **c** can isomerize to the ion−

molecule complex **d** followed by subsequent conversion from **d** to **g**. The difference between path (**b6**) and path (**b7**) is that in path (**b7**) the conversion from **d** to **g** proceeds via the intermediate **l**. Similar to the prevailing of path (**a2**) over path (**a5**), path (**b7**) may be more competitive than path (**b6**).

The formation of the analogous products of (**a**) and (**b**) for the reaction $HSiO^- + CO_2$ was already theoretically studied by Shimizu et al.[5] Their obtained pathways can be written as *path* (***a***) (***R***) → ***c*** → ***j*** → ***q*** → (***a***) $HSiO_2^-$ + *CO* and *path* (***b***) (***R***) → ***a*** → ***h*** → (***b***) HCO_2^- + *SiO*. Notice that in the above and later discussions, the structures for the reaction $HSiO^- + CO_2$ calculated by Shimizu et al.[5] are labeled in italics in order to distinguish from those for the reaction $HSiO^- + CS_2$ in our paper. Their obtained structures ***a***, ***j***, ***h***, and ***q*** are analog of **v**, **c**, **g′**, and **i** in the present paper. A minor difference between *path* (***a***) and our path (**a11**) is that Shimizu et al. located an ion−molecule complex ***c*** between the reactant (***R***) and the three-membered ring ***j***. However, we fail to locate the ***c*** analogue for the reaction $HSiO^- + CS_2$ at the B3LYP/6-311++G(d,p) level. Actually, in Shimizu et al.'s paper, the barrier from ***c*** to ***j*** is just 0.1 kcal/mol at the MP2(full)/6-31++G(d,p) level and the value is further reduced to −0.1 kcal/mol at the single-point MP4/6-311++G(d,p) level.[5] This indicates that the three-membered ring structure ***j*** may be formed almost with no barrier for the reaction $HSiO^- + CO_2$, and so may be **c** for the reaction $HSiO^- + CS_2$. *Path* (***b***) by Shimizu et al.[5] is completely analogous to path (**b1**) in this paper. Note that we locate another pathway (**R**) → **a** → **g** → (**b**) that is also included in path (**b1**). The analogues of the other pathways, i.e., path (**a1**, **a2**, **a5**) and path (**b6**, **b7**), however, were not considered by Shimizu et al.[5] As discussed above, these pathways should not be neglected for the reaction $HSiO^- + CS_2$. Actually, the analogy of path (**a1**) was previously suggested for the formation of oxygen-transfer product (***a***) by Gronert et al.[2] for the reaction $HSiO^- + CO_2$. Yet, it was later excluded on the basis of their isotope labeling experiment.[2]

Shimizu et al.[5] also considered the possibility of forming product (***a***) for the reaction $HSiO^- + CO_2$ via the four-membered ring structure. Their calculated pathway is (***R***) → ***a*** (***b***) → ***i*** → ***q*** → (***a***). The species ***b*** (ion−molecule complex) and ***i*** (four-membered ring structure) are analogous to **b** and **e** in this paper. Their calculated transition state ***m*** connecting ***i*** and ***q*** is 21.1 kcal/mol higher than the reactant.[5] Thus they concluded that the formation of (***a***) via the four-membered ring structure ***i*** is energetically not allowed. For the reaction $HSiO^- + CS_2$, we fail to optimize the analogous transition state between the four-membered ring structure **e** and the ion−molecule complex **j** at the B3LYP/6-311++G(d,p) level. Fortunately, at the MP2/6-311++G(d,p) level, such a transition state (**TSej***) is obtained. At the single-point B3LYP level using the MP2-optimized geometry, the energy of **TSej*** is equal to that of the reactant. This indicates that, similar to the reaction $HSiO^- + CO_2$, the pathway involving the direct CS extrusion transition state **TSej*** to form product (**a**) is also energetically unfavorable for the reaction $HSiO^- + CS_2$. However, the formation of product (**a**) is actually energetically allowed via complex pathways involving the four-membered ring structure **e**, i.e., path (**a8**, **a9**, **a10**). Certainly, the three pathways cannot compete with the four more feasible pathways path (**a1**, **a2**, **a5**, **a11**) since the kinetically quite unstable species **m** is involved.

3.2.2. Formation of (c) $HSiS^-$ + COS, (d) $HCOS^-$ + SiS, and (e) $HSiS_2^-$ + CO. Now let us turn our attention to the formation channels for the three products (**c**) $HSiS^-$ + COS, (**d**) $HCOS^-$ + SiS, and (**e**) $HSiS_2^-$ + CO. Although they are lower in energy than (**a**) and (**b**), they were not observed in Gronert et al.'s experiment.[2] Formally, the three products are associated with oxygen−sulfide exchange, oxygen−sulfide exchange and hydride-transfer, and oxygen−sulfide exchange and sulfide-transfer processes, respectively. From the PES in Figure 3, we can obtain the energetically allowed pathways for the three products, i.e., 23 pathways for product (**c**), 14 for product (**d**), and 7 for product (**e**) as shown in Figures 6, 7, and 8, respectively.

Of the 23 pathways for the oxygen−sulfide exchange product (**c**), nearly all are associated with one or more of the three species **f**, **h**, and **m** except path (**c13**). As discussed in section 3.3.1, the most leading product that the three species may lead to is the lowest-lying product (**e**). Thus, path (**c13**), which involves two ion−molecule complexes **b** and **k** and one four-membered ring structure **e**, is the exclusive more feasible pathway to form the oxygen−sulfide exchange product (**c**) for the reaction $HSiO^- + CS_2$. This is similar to the situation for the reaction $HSiO^- + CO_2$ calculated by Shimizu et al.[5]

There are altogether 14 energetically allowed reaction pathways for product (**d**). Among them, nine pathways path (**d3**, **d4**, **d6**, **d7**, **d8**, **d9**, **d12**, **d13**, **d14**) are associated with the three low-lying yet kinetically unstable species **f**, **h**, and **m**. Thus, their contribution to the formation product (**d**) seems quite insignificant. Among the remaining five ones, path (**d1**) and path (**d2**) are concerned with the initial ion−molecule intermediate **a** or **v**. In addition, two low-lying and kinetically stable ion−molecule species **g** (or **g′**), **d**, and **l** are involved in both pathways. It is clear that path (**d1**) may be more competitive than path (**d2**) owing to the lower energy of **TSgl** than that of **TSdg**. Besides two kinetically unstable ion−molecule complexes **b** and **k**, there are two low-lying and kinetically stable species **e** (four-membered ring) and **u** (ion-molecule) involved in path (**d5**). For path (**d10**) and path (**d11**), the three-membered ring structures **c** and the ion−molecule complexes **d**, **g**, and **l** are related. Certainly, path (**d10**) may be more competitive than path (**d11**) since **TSdl** in the former pathway is 6.3 and 2.4 kcal/mol lower than **TSdg** and **TSgl** in the latter, respectively. All the five pathways path (**d1**, **d2**, **d5**, **d10**, **d11**) are feasible to form product (**d**). However, of the five feasible pathways, it is still difficult to ascertain their contribution to product (**d**) since these pathways involve different initially formed structures. For example, we are unable to determine the contribution between path (**d5**) involving the three-membered ring structure **c** and path (**d1**) and path (**d2**) involving the ion-molecule complex **a** or **v**.

It is interesting to find that all the seven pathways path (**e1**, **e2**, **e3**, **e4**, **e5**, **e6**, and **e7**) are responsible for the formation of the lowest-lying product (**e**). Starting from the reactant (**R**), product (**e**) can be formed via various reaction pathways involving all the four initially formed species **a**, **b**, **c**, and **v** and the final low-lying yet kinetically unstable structure **m**. The former four pathways are related to the ion−molecule complexes **a** and **v**. Since **TSgl** is somewhat lower than **TSdg**, path (**e3**) and path (**e4**) may be more competitive than path (**e1**) and path (**e2**). Surely, path (**e1**) and path (**e3**) are less competitive than path (**e2**) and path (**e4**), respectively, since the conversion barrier for **d** → **c** is 9 kcal/mol higher than that for **d** → **t**. Path (**e5**) is a pathway that is related to two four-membered ring structures **e** and **q** and three ion−molecule complexes **b**, **k**, and **m**. The latter path (**e6**) and path (**e7**) are related to the three-membered ring structure **c**. Of course, path (**e6**) is more competitive than

path (**e7**) since the barrier from **c** to **f** is 5.3 kcal/mol lower than that from **c** to **d**. Again, the contribution of the pathways involving different initially formed intermediates to product (**e**) is difficult to anticipate.

3.3. Mechanism for the Reaction $HSiO^- + CS_2$. Now let us discuss the overall mechanism of the reaction $HSiO^- + CS_2$. In section 3.2, we know that the potential energy surface of this reaction is very complex. Once the reaction is initiated, five energetically low-lying products (**a**) $HSiOS^- + CS$, (**b**) $HCS_2^- + SiO$, (**c**) $HSiS^- + COS$, (**d**) $HCOS^- + SiS$, and (**e**) $HSiS_2^- + CO$ can be obtained via various feasible and more feasible reaction pathways. For simplicity, we only make comparisons between these more feasible pathways of the five products presented in Figures 4, 5, 6, 7, and 8 with an attempt to obtain the most possible products that the four initially formed structures **a**, **b**, **c**, and **v** may lead to. On the basis of the energetics of various intermediates and transition states as listed in Table 1, we can readily see that the species **a** and **v** may most possibly lead to product (**b**) via path (**b1**) **R** → **a** (**v**) → **g** (**g′**) → (**b**), **b** to product (**c**) via path (**c13**) **R** → **b** → **e** → **k** → (**c**) or to product (**d**) via path (**d5**) **R** → **b** → **e** → **k** → **u** → (**d**), and **c** to product (**e**) via path (**e6**) **R** → **c** → **f** → **h** → **m** → (**e**). Notice that path (**d1**) **R** → **a** (**v**) → **g** (**g′**) → **l** → (**d**) may be just a little less competitive than path (**b1**) since the barrier from **g** to **l** is only 1.5 kcal/mol higher in energy than that from **g** to (**b**). We also note that although the barrier from **k** to **u** in path (**d5**) is 1.3 kcal/mol lower than that from **k** to (**c**) in path (**c13**), the two pathways can only be considered as competitive owing to the existence of a large barrier 28.4 kcal/mol from **u** to (**d**). If only these most feasible pathways, which may contribute most to the corresponding products, are taken into consideration, then the formation of the products (**b**), (**c**), (**d**), and (**e**) can be described as via ion−molecule complex, four-membered ring, four-membered ring, and three-membered ring mechanisms, respectively. Note that the four-membered ring mechanism of the oxygen−sulfide exchange product (**c**) for the reaction $HSiO^- + CS_2$ is completely analogous to that for the reaction $HSiO^- + CO_2$ calculated by Shimizu et al.[5] However, it is difficult to determine the dominant pathway leading to product (**a**).

Now it is clear that for the reaction $HSiO^- + CS_2$ all five products (**a**), (**b**), (**c**), (**d**), and (**e**) can be formed both thermodynamically and kinetically. This implies that extensive oxygen−sulfide exchange accompanied with sulfide- or hydride-transfer occurs for this reaction. A further discussion on the relative abundance of the five products for the reaction $HSiO^- + CS_2$ simply by comparison of the reaction pathways may also be useful. Surely, without detailed dynamic calculations, the contributions of the four most feasible pathways path (**b1**), path (**c13**), path (**d5**), and path (**e6**) to the respective products (**b**), (**c**), (**d**), and (**e**) are difficult to anticipate. Yet, we still feel that it is reasonable to assume similar contribution of the four pathways to the corresponding products. It is clear that path (**a1**, **a2**, **a5**) cannot compete with path (**b1**), path (**d1**, **d2**), and path (**e1**, **e2**, **e3**, **e4**). Moreover, path (**a11**) cannot compete with path (**b6**, **b7**), path (**d10**), and path (**e6**, **e7**). On the other hand, the products (**b**), (**d**), and (**e**) are 12.2, 15.3, and 52.3 kcal/mol lower than product (**a**), respectively. Thus, both from kinetic and thermodynamical viewpoints, the formation of product (**a**) may be less favorable than that of the products (**b**), (**d**), and (**e**). Path (**d5**) for product (**d**) competes with path (**c13**) for product (**c**). Also, another two pathways path (**d1**, **d2**) contribute to product (**d**). Therefore, product (**d**) may be more than product (**c**). Certainly, path (**e5**) cannot compete with path (**c13**) since **TSkq** and **TSmq** are 3.3 and 8.3 kcal/mol higher than product (**c**). However, other reaction pathways path (**e1**, **e2**, **e3**, **e4**, **e6**, **e7**) also contribute to product (**e**) among which path (**e6**) may be competitive with path (**c13**). Thus, product (**e**) may still be more than product (**c**). Similarly, product (**b**) may be more abundant than product (**c**). The relative abundance between the products (**a**) and (**c**) and between (**b**), (**d**), and (**e**), however, is difficult to anticipate. We may expect that of the final product distributions, the relative branching ratios of the products (**a**) and (**c**) should not make significant differences, and such is the case with (**b**), (**d**), and (**e**).

3.4. Comparison with the Experimental Results. The ion−molecule reaction $HSiO^- + CS_2$ was already experimentally studied by Gronert et al.[2] They observed two dissociation products (**a**) $HSiOS^- + CS$ and (**b**) $HCS_2^- + SiO$ with the branching ratio of 3:7. Their results showed no indication of the formation of any oxygen−sulfide exchange product for the reaction $HSiO^- + CS_2$. However, our calculations show that in addition to the observed products (**a**) and (**b**), the other energetically more low-lying products (**c**) $HSiS^- + COS$, (**d**) $HCOS^- + SiS$, and (**e**) $HSiS_2^- + CO$ should also be observable owing to both thermodynamical and kinetic reasons. Our calculated results also indicate that the relative abundance of the three unobserved low-lying products (**d**) and (**e**) may be more than that of product (**a**) and be comparable to that of product (**b**). On the other hand, in the isotopically labeled experiment for the reaction $HSi^{18}O^- + CO_2$,[2] extensive oxygen−oxygen exchange between $HSi^{18}O^-$ and CO_2 was observed to form five labeled and unlabeled anions, i.e., $HSi^{16}O^-$, $HSi^{18}O^{16}O^-$, $HSi^{16}O_2^-$, $HC^{18}O^{16}O^-$, and $HC^{16}O_2^-$. Clearly, the five anions $HSiS^-$, $HSiOS^-$, $HSiS_2^-$, $HCOS^-$, and HCS_2^- in the respective products (**c**), (**a**), (**e**), (**d**), and (**b**) for the reaction $HSiO^- + CS_2$ are parallel to those in the products for the labeled reaction $HSi^{18}O^- + CO_2$. It is interesting that our predicted products for the reaction $HSiO^- + CS_2$ and the experimentally observed ones for the isotopically labeled reaction $HSi^{18}O^- + CO_2$ are parallel. Our calculations imply that despite the electronegativity difference between oxygen and sulfide, there may be more similarities than discrepancies between the two reactions of $HSiO^-$ with CO_2 and CS_2. Therefore, we feel that further detailed experiments are in great need to clarify the mechanism of the ion−molecule reaction $HSiO^- + CS_2$.

It is worthy of note that the anion $HSi^{16}O_2^-$ could not be predicted by the calculated potential energy surface of the reaction $HSiO^- + CO_2$ by Shimizu et al.[5] Our calculations for the reaction $HSiO^- + CS_2$ may give some beneficial implications to interpret the formation of this anion for the labeled reaction $HSi^{18}O^- + CO_2$. Moreover, the SIFT experiments on the other analogous ion−molecule reactions such as CH_3SiO^-, CH_3OSiO^-, $HSiS^-$, and $HSiNH^-$ with CO_2, CS_2, and COS were carried out by Damrauer et al.[3,4] For all of these reactions, the products associated with atom-transfer and atom−atom exchange processes were observed. Our calculated potential energy surface of the reaction $HSiO^- + CS_2$ may represent a useful model to understand the mechanisms for these important low-valent silicon-containing ion−molecule reactions.

3.5. Reliability of the B3LYP Method for $HSiO^- + CS_2$ Reaction. Since the present system for the reaction **$HSiO^- + CS_2$** contains the second-row elements Si and S, it is very desirable to assess the reliability of the B3LYP/6-311++G(d,p) method for the calculated property. We are mainly concerned about the use of this method for the reaction exothermicity and especially the interconversion barrier heights.

TABLE 2: Total (in au) and Relative (in kcal/mol) Energies of the Species (R), (a), (b), (c), (d), (e), a, c, TSai, and TScd Calculated Using the B3LYP Method with 6-311++G(d,p), aug-cc-pVDZ, aug-cc-pVTZ Basis Sets, the MP2 Method with 6-311++G(d,p) and aug-cc-pVDZ Basis Sets, and the CCSD(T) Method with aug-cc-pVDZ Basis Set

	B3LYP			MP2		CCSD(T)
species	/6-311++G(d,p)	/aug-cc-pVDZ	/aug-cc-pVTZ	/6-311++G(d,p)	/aug-cc-pVDZ	/aug-cc-pVDZ
(R) $HSiO^- + CS_2$	−1199.942 784 (0.0)	−1199.900 412 (0.0)	−1199.977 537 (0.0)	−1198.035 814 (0.0)	−1198.030 161 (0.0)	−1198.091 942 (0.0)
(a) $HSiOS^- + CS$	−1199.960 270 (−11.0)	−1199.918 489 (−11.3)	−1199.996 458 (−11.9)	−1198.054 349 (−11.6)	−1198.054 750 (−15.4)	−1198.122 306 (−19.1)
(b) $HCS_2^- + SiO$	−1199.983 404 (−25.5)	−1199.942 183 (−26.2)	−1200.015 992 (−24.1)	−1198.073 638 (−23.7)	−1198.073 685 (−27.3)	−1198.138 467 (−29.2)
(c) $HSiS^- + COS$	−1199.982 720 (−25.1)	−1199.947 788 (−29.7)	−1200.015 570 (−23.9)	−1198.062 700 (−16.9)	−1198.071 118 (−25.7)	−1198.138 733 (−29.4)
(d) $HCOS^- + SiS$	−1199.988 875 (−28.9)	−1199.955 767 (−34.7)	−1200.020 414 (−26.9)	−1198.067 563 (−19.9)	−1198.067 563 (−23.5)	−1198.147 975 (−35.2)
(e) $HSiS_2^- + CO$	−1200.044 371 (−63.7)	−1200.008 249 (−67.7)	−1200.078 646 (−63.4)	−1198.130 641 (−59.5)	−1198.141 308 (−69.7)	−1198.208 731 (−73.3)
a	−1199.953 624 (−6.8)	−1199.911 654 (−7.1)	−1199.988 739 (−7.0)	−1198.041 980 (−3.9)	−1198.039 288 (−5.7)	−1198.099 654 (−4.8)
TSai[a]	−1199.946 418 (−2.3) [4.5]	−1199.905 865 (−3.4) [3.7]	−1199.982 371 (−3.0) [4.0]	−1198.034 859 (+0.6) [4.5]	−1198.034 565 (−2.8) [2.9]	−1198.099 803 (−4.9) [−0.1]
c	−1200.013 550 (−44.4)	−1199.960 260 (−37.6)	−1200.039 354 (−38.8)	−1198.100 459 (−40.6)	−1198.096 946 (−41.9)	−1198.157 649 (−41.2)
TScd[b]	−1199.962 648 (−12.5) [*31.9*]	−1199.918 631 (−11.4) [*26.2*]	−1199.998 531 (−13.2) [*25.6*]	−1198.048 444 (−7.9) [*32.7*]	−1198.047 867 (−11.1) [*30.8*]	−1198.111 851 (−12.5) [*28.7*]

[a] The values in brackets are barrier heights for **a** → **i** conversion in kcal/mol. [b] The italic values in brackets are barrier heights for **c** → **d** conversion in kcal/mol.

Here, we choose 10 illustrative species, i.e., the reactant (**R**), the five dissociation products (**a**), (**b**), (**c**), (**d**), and (**e**), the loosely bonded ion−molecule intermediate **a**, the kinetically stable three-membered ring intermediate **c**, and the two transition states **TSai** and **TScd**. These species either contain multiply bonding species (**R**), (**a**), (**b**), (**c**), (**d**), (**e**), **a**, and **c** or contain weakly bonding species **a**, **TSai**, and **TScd**, and the extent of electron correlation and basis set influences may be well-reflected.

For comparison of the energetics, we carry out the single-point calculations using the B3LYP method with standard 6-311++G(d,p), Dunning's correlation consistent aug-cc-pVDZ and aug-cc-pVTZ basis sets, the MP2 method with 6-311++G-(d,p) and aug-cc-pVDZ basis sets, and the CCSD(T) method with aug-cc-pVDZ basis set. Further calculations such as MP2/aug-cc-pVTZ and CCSD(T)/aug-cc-pVTZ are not performed owing to the limited computation resources. The total and relative energies with reference to the reactant (**R**) are listed in Table 2. Note that the zero-point energies at the B3LYP/6-311++G(d,p) level are not included. First, we can readily find that at the B3LYP level with 6-311++G(d,p), aug-cc-pVDZ, and aug-cc-pVTZ basis sets, the relative energies for each of the 10 representative species are close. The B3LYP/6-311++G-(d,p) values are even in excellent agreement with the B3LYP/aug-cc-pVTZ values within 2 kcal/mol except for structure **c**. However, the discrepancies between the MP2/6-311++G(d,p) and MP2/aug-cc-pVDZ relative energies are relatively much larger. This indicates that the basis set effect may be less significant for the B3LYP method than for MP2. Second, the relative energies for fragments (**R**), (**a**), (**b**), (**c**), (**d**), and (**e**) at both B3LYP and MP2 levels with various basis sets are lower than those at the CCSD(T)/aug-cc-pVDZ level with the largest deviation 9.6 kcal/mol for (**e**). However, the relative energies for the intermediates and even for transition states are very close at the B3LYP, MP2, and CCSD(T) levels, and the agreement of B3LYP with CCSD(T) is better than that of MP2 with CCSD-(T). Also, as shown in Table 2, the predicted B3LYP/6-311++G(d,p) barrier heights 4.5 (**a** → **i**) and 31.9 (**c** → **d**) kcal/mol are very close to the MP2/6-311++G(d,p) (4.5 and 32.7 kcal/mol), MP2/aug-cc-pVDZ (2.9 and 32.8 kcal/mol), and CCSD(T)/aug-cc-pVDZ (−0.1 and 28.7 kcal/mol) values. Notice that the sign of the **a** → **i** conversion barrier is negative, indicating a very small and maybe even zero activation energy. Third, the MP2 method with both 6-311++G(d,p) and aug-cc-pVDZ basis sets fails to predict the relative energy order between the species (**b**) and (**d**) while the B3LYP method does. Moreover, the MP2/6-311++G(d,p) relative energy of **TSai** is 0.6 kcal/mol above that of (**R**), which may possibly lead to the incorrect conclusion that reaction pathways involving the transition state **TSai** are not feasible.

Anyhow, for the 10 representative species, the B3LYP/6-311++G(d,p) method is able to predict satisfactory results in comparison with the CCSD(T)/aug-cc-pVDZ method and works better than MP2 since MP2 fails to predict the correct energy order between the products (**b**) and (**d**). Particularly, since both the relative energies and interconversion barrier heights for the representative species at the B3LYP/6-311++G(d,p) level are very close to the CCSD(T)/aug-cc-pVDZ values, we expect that our B3LYP/6-311++G(d,p) calculations may be reliable for investigation of the whole PES of the reaction $HSiO^- + CS_2$, in which a number of intermediates and transition states are involved. Moreover, since the B3LYP/6-311++G(d,p) (242) method is much less expensive than the B3LYP/aug-cc-pVDZ (662), B3LYP/aug-cc-pVTZ (5834), MP2/6-311++G(d,p) (346), MP2/aug-cc-pVDZ (1833), and CCSD(T)/aug-cc-pVDZ (8444) methods, we feel that performance of the B3LYP/6-311++G-(d,p) calculations is very economical for the present reaction $HSiO^- + CS_2$. Note that the values in parentheses are CPU time in seconds for a single-point energy calculation carried out at the HP9000 series of mini-supercomputer N4000 with six CPUs.

4. Conclusions

The detailed potential energy surface of the reaction $HSiO^- + CS_2$ is investigated by means of the B3LYP/6-311++G(d,p) method to explore the mechanism for the formation of five low-lying products (**a**) $HSiOS^- + CS$, (**b**) $HCS_2^- + SiO$, (**c**) $HSiS^- + COS$, (**d**) $HCOS^- + SiS$, and (**e**) $HSiS_2^- + CO$. It is shown that each of the five products can be

produced both thermodynamically and kinetically via a variety of reaction pathways involving the ion−molecule complexes and three-membered ring and four-membered ring structures. Therefore, all the five products are experimentally observable, indicative of extensive oxygen−sulfide exchange for the reaction $HSiO^- + CS_2$. Our calculations are in sharp contradiction to the experimental results that only the products (**a**) and (**b**) were observed for the reaction $HSiO^- + CS_2$, yet are in harmony with the isotopically labeled reaction $HSi^{18}O^- + CO_2$. Our results suggest that future mechanistic experimental studies on the reaction $HSiO^- + CS_2$ are still in need to identify the three low-lying products (**c**), (**d**), and (**e**), which are still experimentally unknown for this reaction. Moreover, the results presented in this paper may provide some useful information for other analogous ion−molecule reactions such as CH_3SiO^-, CH_3OSiO^-, $HSiS^-$, and $HSiNH^-$ with CO_2, COS, and CS_2.

Acknowledgment. This work is supported by the National Natural Science Foundation of China.

References and Notes

(1) Damrauer, R.; Hankin, J. A. *Chem. Rev.* **1995**, *95*,1137.

(2) Gronert, S.; O'Hair, R. A. J.; Prodnuk, S.; Sülzle, D.; Damrauer, R.; DePuy, C. H. *J. Am. Chem. Soc.* **1990**, *112*, 997.

(3) Damrauer, R.; Krempp, M. *Organometallics* **1990**, *9*, 999.

(4) Damrauer, R.; Krempp, M.; O'Hair, R. A. J. *J. Am. Chem. Soc.* **1993**, *115*, 1998.

(5) Shimizu, H.; Gordon, M. S.; Damrauer, R.; O'Hair, R. A. J. *Organometalics* **1995**, *14*, 2664.

(6) (a) Frisch, M. J.; Trucks, G. W.; Schlegel, H. B.; Gill, P. M. W.; Johnson, B. G.; Robb, M. A.; Cheeseman, J. R.; Keith, T.; Petersson, G. A.; Montgomery, J. A.; Raghavachari, K.; Al-Laham, M. A.; Zakrzewski, V. G.; Ortiz, J. V.; Foresman, J. B.; Cioslowski, J.; Stefanov, B. B.; Nanayakkara, A.; Challacombe, M.; Peng, C. Y.; Ayala, P. Y.; Chen, W.; Wong, M. W.; Andres, J. L.; Replogle, E. S.; Gomperts, R.; Martin, R. L.; Fox, D. J.; Binkley, J. S.; Defrees, D. J.; Baker, J.; Stewart, J. P.; Head-Gordon, M.; Gonzalez, C.; Pople, J. A. *Gaussian 94*, Revision E.2; Gaussian, Inc.: Pittsburgh PA, 1995. (b) Frisch, M. J.; Trucks, G. W.; Schlegel, H. B.; Scuseria, G. E.; Robb, M. A.; Cheeseman, J. R.; Zakrzewski, V. G.; Montgomery, J. A.; Stratmann, Jr., R. E.; Burant, J. C.; Dapprich, S.; Millam, J. M.; A Daniels, D.; Kudin, K. N.; Strain, M. C.; Farkas, O.; Tomasi, J.; Barone, V.; Cossi, M.; Cammi, R.; Mennucci, B.; Pomelli, C.; Adamo, C.; Clifford, S.; Ochterski, J.; Petersson, G. A.; Ayala, P. Y.; Cui, Q.; Morokuma, K.; Malick, D. K.; Rabuck, A. D.; Raghavachari, K.; Foresman, J. B.; Cioslowski, J.; Ortiz, J. V.; Stefanov, B. B.; Liu, G.; Liashenko, A.; Piskorz, P.; Komaromi, I.; Gomperts, R.; Martin, R. L.; Fox, D. J.; Keith, T.; Al-Laham, M. A.; Peng, C. Y.; Nanayakkara, A.; Gonzalez, C.; Challacombe, M.; Gill, P. M. W.; Johnson, B.; Chen, W.; Wong, M. W.; Andres, J. L.; Gonzalez, C.; Head-Gordon, M.; Replogle, E. S.; Pople, J. A. *Gaussian 98*, Revision A.6; Gaussian, Inc.: Pittsburgh PA, 1998.